Modeling ion transport across thin-film composite membranes during saltwater electrolysis

Rachel F. Taylor[1], Xuechen Zhou[1], Chenghan Xie[1], Fernan Martinez[3], Xinran Zhang[1], Bastiaan Blankert[3], Cristian Picioreanu[3,4], Bruce E. Logan[1,2*]

[1]Department of Chemical Engineering, The Pennsylvania State University, University Park, PA, 16801, USA.
[2]Department of Civil and Environmental Engineering, The Pennsylvania State University, University Park, PA, 16801, USA.
[3]Water Desalination and Reuse Center, Biological and Environmental Science and Engineering Division, King Abdullah University of Science and Technology, Thuwal, 23955, Saudi Arabia
[4]Environmental Science & Engineering Program, King Abdullah University of Science and Technology, Thuwal, 23955, Saudi Arabia

*Corresponding author. Email: blogan@psu.edu; Tel.: +1-814-863-7908

ABSTRACT

Affordable thin-film composite (TFC) membranes are a potential alternative to more expensive ion exchange membranes in saltwater electrolyzers used for hydrogen gas production. We used a solution-friction transport model to study how the induced potential gradient controls ion transport across the polyamide (PA) active layer and support layers of TFC membranes during electrolysis. The set of parameters was simplified by assigning the same size-related partition and friction coefficients for all salt ions through the membrane active layer. The model was fit to experimental ion transport data from saltwater electrolysis with 600 mM electrolytes at 10 mA cm^{-2}. When the electrolyte concentration and current density were increased, the transport of major charge carriers was successfully predicted by the model. Ion transport calculated using the model only minimally changed when the negative active layer charge density was varied from 0 to 600 mM, indicating active layer charge was not largely responsible for controlling ion crossover during electrolysis. Based on model simulations, a sharp pH gradient was predicted to occur within the supporting layer of the membrane. These results can help guide membrane design and operation conditions in water electrolyzers using TFC membranes.

Key Words: green hydrogen production; solution-friction modeling; Donnan partitioning; polyamide membrane; seawater electrolysis

Synopsis: With minimal fitting parameters, Nernst-planck modeling fit to replicate ion transport data from saltwater electrolysis with an affordable thin-film composite membrane can provide insights into salt and water ion transport for future membrane optimization.

INTRODUCTION

Most current methods of hydrogen production use fossil fuels and release carbon dioxide as a byproduct to the atmosphere, but a sustainable alternative is to use renewable electricity to electrolyze water.[1-3] High capital costs associated with the membrane and catalyst in the electrolyzer, as well as the system's dependence on ultrapure water, are slowing implementation

of this method of green hydrogen production.[4, 5] Directly electrolyzing saltwater would eliminate capital and operating costs associated with water purification currently required for electrolysis.[6, 7] In practice, a major challenge that arises during the direct electrolysis of seawater is chloride ions abundant in saltwater can react at the anode to form chlorine gas, which can be further oxidized to form species that damage electrolyzer components.[8, 9] Avoiding or minimizing Cl^- /Cl_2 reactions at the anode and identifying affordable electrolyzer components will improve the viability of saltwater electrolysis for green hydrogen production.

A new approach to avoid chlorine generation in hydrogen production with a saltwater catholyte is based on using relatively inexpensive thin-film composite (TFC) membranes and a contained, non-reactive anolyte.[8] These membranes possess a thin, size-selective active layer that minimizes migration of chloride ions from the saltwater catholyte to the anode. The active layer is a polyamide (PA) film which is formed via interfacial polymerization onto a support layer of polysulfone, which is normally affixed to polyester web for additional mechanical support.[10] Initial tests showed that using different TFC membranes impacts electrolyzer performance, but some TFC membranes can produce current densities with applied potentials comparable to those needed with more expensive cation exchange membranes (CEMs).[8] Modifications to the membrane have been proposed to decrease the overall resistance of the membrane while reducing chloride permeation, but these studies demonstrate the mechanisms governing the TFC membrane-based electrolyzer performance are not straightforward.[11-13] The multiple composite layers of the membrane have different transport properties, and the size-exclusive nature of the active layer causes the resistance of the membrane to change depending on the abundance of varying ions in solution.

The purpose of this study was to determine whether a simplified Solution-Friction (SF) model could be used to predict transport of the main charge carriers across a TFC membrane during saltwater electrolysis. Modeling has been valuable in deepening our understanding of ion transport across PA TFC membranes during reverse osmosis (RO) and nanofiltration (NF) processes.[14-19] For NF applications there is a large water flux and no external applied electric field, which are conditions much different from those in water electrolyzers. Because this kind of model has never been used to represent ion transport across TFC membranes during saltwater electrolysis quantitatively, it was unknown whether all the typical parameters needed to describe water flux and ion transport for RO applications are largely influential during water electrolysis (WE) applications. A reduced model was developed here to predict ion transport under conditions relevant to WE, by assigning the same size-related partitioning and frictional coefficients to every salt ion. The model was tested under non-steady conditions to observe the dynamic response of the system to large pH changes due to the water splitting reactions. Model calibration was based on using standard salt ion and membrane parameters and fitting four other parameters using ion transport data from electrolysis experiments conducted with electrolytes at a concentration of 600 mM and a set current density of 10 mA cm^{-2}. The utility of this calibrated model was then demonstrated by comparing the predicted ion transport at varying electrolyte concentrations and current densities with our experimental data. We used the validated model to estimate how ion transport rate and selectivity might change during electrolysis for various membrane charge densities. Finally, we examined the formation of steep pH gradients within the membrane layers, due to water ion association from H^+ and OH^- generated at the electrodes.

METHODS

Materials and chemical information

ACS grade $NaClO_4$ and KNO_3 (Sigma-Aldrich) were used as the anolyte and catholyte, respectively, in all electrolysis experiments. All solutions were prepared using deionized (DI) water (>18.2 MΩ cm, Mili-Q ultrapure water purification system, Synergy). SW30XLE membranes (Dow Chemical) were used for all electrolysis experiments. To fully wet the TFC membranes, they were placed in 25% v/v isopropanol aqueous solution on a shaker for 60 minutes. Finally, the membranes were thoroughly rinsed with DI water three times on a shaker for 30 minutes and stored in DI water at 4°C prior to use.

Electrode preparation method

Electrodes were prepared as previously described.[8, 11] The anode and cathode were circular with the same exposed area as the membrane (7.1 cm^2) to enable the electric field to be more evenly distributed across the membrane. Carbon paper was first immersed in a 3/2 v/v ratio of HNO_3/H_2SO_4 for 60 minutes to clean the carbon through oxidation and increase the adhesion of catalyst particles.[20] The carbon paper was then thoroughly rinsed with DI water until the pH of the DI water running off the carbon paper was neutral, and then it was dried in air overnight. For each 7.1 cm^2 electrode, 35.5 mg of 10% Pt/C powder, 29 μL of DI water, 237 μL of a perfluorinated resin solution with 5 wt. % Nafion (Sigma Aldrich), and 118 μL of isopropanol were mixed and painted onto the carbon paper using a brush. The electrodes were dried in air over night before they were used.

Saltwater electrolysis

Two cylindrical reactor chambers, each with a volume of 31 mL, were held together with screws and bolts with an RO membrane positioned between them, as previously described.[8, 11] The anode and cathode were fixed 4 cm away from the membrane at either end of the reactor chambers to ensure bubble formation did not influence ion transport near the membrane (Figure 1a, Figure S1 and S2). Both the anolyte ($NaClO_4$) and catholyte (KNO_3) were mixed with an overhead stirrer (Caframo) at a rate of 100 rpm. Unlike chloride, NO_3^- cannot be oxidized at the anode to compete with the oxygen evolution reaction OER. Additionally, NO_3^- and Cl^- are both monovalent and have similar hydrated radii.[21] Therefore, NO_3^- was used as counter-ion in place of Cl^-, to facilitate an accurate measurement of anion concentration transported from catholyte to anolyte. A VMP3 potentiostat (Biologic) was used to apply the set current density to the cell. Samples (0.5 mL) were collected from both the anolyte and catholyte every 20 minutes, resulting in a total volume change of 3 mL in each chamber over the course of an experiment. The experiments were stopped after 120 minutes to avoid a large water volume change in the reactor and maintain constant working membrane and electrode area. Additionally, using a 120-minute experimental period enabled us to examine both the dynamic changes of the system when the pH is rapidly decreasing in the anolyte and increasing in the catholyte as well as relatively stable operation. Previous saltwater electrolysis studies with TFC membranes demonstrated that a pseudo steady-state in pH was reached after a 60 minute period, so 120 minutes was chosen here to ensure both periods of rapidly changing and relatively stable pH conditions.[8] The samples were diluted 10-fold prior to analysis using an ion chromatograph (Integrion Ion Chromatography system, Thermo Fisher). The pH of the diluted samples was measured using a pH probe (SevenMulti, Mettler Toledo, Switzerland) which was calibrated prior to measurements. Electrolysis experiments were conducted in duplicate.

Fraction of charge carried

The fraction of charge carried across the membranes by salt ions (Na^+, NO_3^-, K^+, ClO_4^-) and water ions (H^+, OH^-) was calculated using the transport results at the set current density (detailed calculations in S1). The constant current density i_a provides a fixed charge flux across the membrane at any given point, with the charge carried by salt ions (Na^+ and NO_3^-) and water ions generated by the electrodes (H^+ and OH^-) moving in the direction of the potential gradient. Salt ions crossing the membrane in the direction opposite of the potential gradient (K^+ and ClO_4^-) increase the amount of charge that must be carried by major ions, such that $i_a = F(|J_{Na^+}| + |J_{NO_3^-}| + |J_{H^+}| + |J_{OH^-}| - |J_{ClO_4^-}| - |J_{K^+}|)$, with J_i the molar flux of any ion i. After calculating the flux of charge carried by salt ions, any remaining charge not accounted for was attributed to water ions.

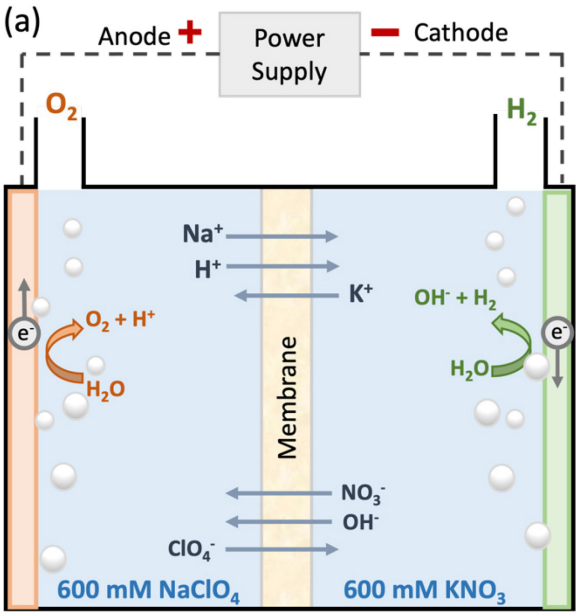

151

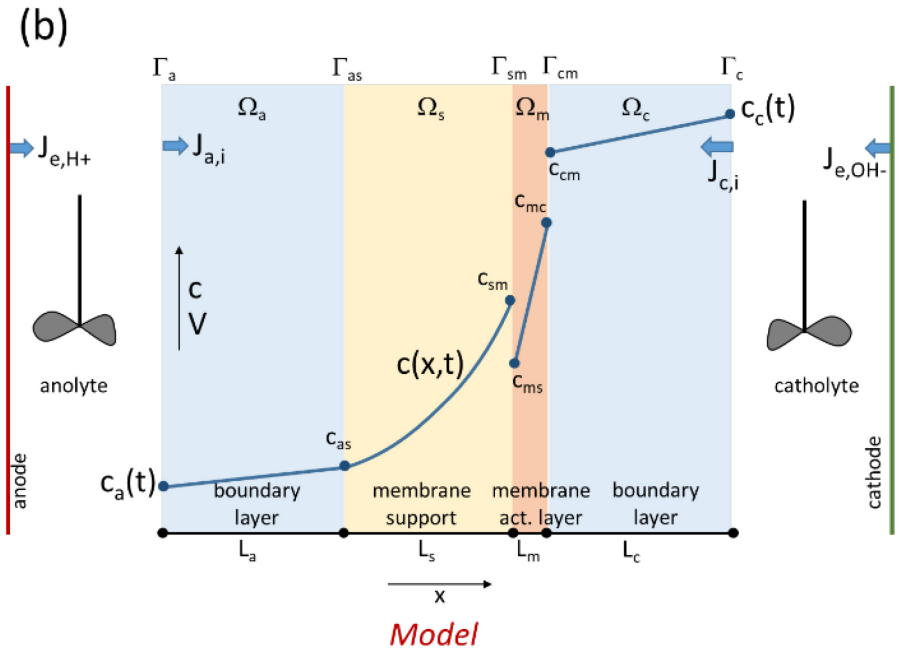

152
153 **Figure 1.** (a) Schematic of saltwater electrolysis cell with anodic and cathodic reactions, and ion
154 transport directions specified; (b) The model breakdown of the two-chamber system into two
155 ideally mixed domains (bulk anolyte and catholyte) and four 1-D domains (two diffusion
156 boundary layers adjacent to the membrane and two membrane layers) with distinct mass
157 transport properties. The system is here not represented to scale. A typical concentration profile
158 (K^+) is represented across the domains Ω, separated by interfaces Γ.
159
160
161

Modeling ion transport in a batch saltwater electrolysis cell

We constructed a time-dependent, one-dimensional (1-D) numerical model to simulate the transport of sodium (Na^+), nitrate (NO_3^-), potassium (K^+), perchlorate (ClO_4^-), protons (H^+), and hydroxide (OH^-) across a TFC membrane within a batch electrolyzer. This numerical framework was implemented in COMSOL Multiphysics v. 6.2 software (www.comsol.com, COMSOL AB, Stockholm, Sweden).

Geometry. The 1-D concentration and potential gradients were calculated across a system with interconnected domains, consistent with the geometry of the experimental batch reactor (Figure 1b). Due to vigorous stirring, the anolyte and catholyte (constant) volumes were assumed ideally mixed, thus represented by one concentration for each ion, $c_{a,i}$ and $c_{c,i}$ - both functions of time. The Pt/C electrodes were represented as sources of H^+ to the anolyte and OH^- to the catholyte. Electrolytes were separated by a TFC membrane situated at a distance L from each electrode. Time-dependent gradients of concentration c_i and potential φ were computed in several layers forming a series of resistances to mass and charge transfer between the anolyte and catholyte. Mass transfer boundary layers (concentration boundary layer, CBL) of equal thickness L_a=L_c were considered in the electrolyte adjacent to either side of the membrane. The TFC membrane consisted of a thin active layer facing the catholyte and porous support layer facing the anolyte. Based on previous studies, the active layer was estimated to be L_m=150 nm thick, and the porous support layer was L_s=150 µm thick.[10, 14, 22]

Ion and charge balances. The time-dependent spatial distribution of ion concentrations c_i and electrolyte potential φ in the four connected layers were computed from material and charge balances. The time-dependent transport of any ion i of charge z_i within the several layers is represented by Nernst-Planck ion fluxes including diffusion and electromigration.[12, 14]

$$\frac{\partial c_i}{\partial t} = f\, D_i \frac{\partial}{\partial x}\left(\frac{\partial c_i}{\partial x} + z_i\, c_i \frac{F}{RT}\frac{\partial \varphi}{\partial x}\right) + r_i \qquad [1]$$

A coefficient f was used to modify the magnitude of the diffusion coefficients D_i in different domains. In the mass transfer boundary layers (domains Ω_a and Ω_c), the diffusion coefficients were those in water (f = 1). In the membrane support layer (Ω_s), where pores are on the micron scale, $f = \varepsilon_s$ as an effectiveness factor lumping porosity and tortuosity effects. In the dense active layer (Ω_m), ion transport is also retarded by friction between ions and the membrane polymer, thus using a smaller factor $f = \varepsilon_a$.[23] Exact values of these effectiveness or friction factors remain highly uncertain, therefore, to simplify the model, the same values ε_s and ε_a were assumed for all six ions and fit to our experimental ion transport data. To compute local pH, water dissociation with equilibrium constant K_w was included in a kinetic way with rate $r_{H^+} = r_{OH^-} = k_w(1 - c_{H^+}c_{OH^-}/K_w)$ where the rate coefficient k_w takes an arbitrarily large value to approximate equilibrium in all domains. There are no reaction rate terms r_i for Na^+, NO_3^-, K^+ and ClO_4^-.

The electroneutrality at every point x in the system is ensured by a charge balance. In electrolyte boundary layers and membrane support, the balance is a sum of concentrations c_i multiplied by ion charge z_i (eq. [2a]). In the membrane active layer, the electroneutrality condition includes the membrane charge density X in molar units, here negatively charged (eq. [2b]).

$$\sum_i z_i c_i = 0 \qquad [2a]$$

$$-X + \sum_i z_i c_i = 0 \qquad [2b]$$

In every experiment, the membrane active layer faced the catholyte. Because the catholyte pH rapidly becomes highly alkaline (pH~13) during electrolysis under these test conditions in previous studies [8], the carboxylic groups on the polyamide will be deprotonated, fully functionalizing the active layer. The negative active layer charge density was set to X=400 mM to be consistent with the highly alkaline operating conditions.[24] The differential-algebraic system of equations contains six ion balances (eq. [1]) and one charge balance (eq. [2]) in all domains, and - after assigning boundary and initial conditions - allows computing the 6 concentrations c_i and one electrolyte potential φ.

Boundary conditions. On the bulk anolyte and catholyte boundaries (Γ_a and Γ_c), concentrations $c_{a,i}$ and $c_{c,i}$ were set. These bulk concentrations result from solving a system of differential equations in the batch system in time with constant volume (eq. [3]).

$$\frac{dc_{a,i}}{dt} = \frac{A}{V}\left(J_{a,i} - J_i\right) + r_i, \qquad \frac{dc_{c,i}}{dt} = \frac{A}{V}\left(J_{c,i} + J_i\right) + r_i \qquad [3]$$

A source flux accounts for H^+ production at anode, equal with the flux of OH^- produced at the cathode, $J_{a,H+} = J_{c,OH-} = i_a/F$ while no other ions are interacting with the electrodes, thus $J_{a,i} = 0$ for all other ions. Another total flux J_i, (i.e., diffusion + migration), is exchanged with the corresponding boundary layers for all ions. Kinetic rates $r_{H^+} = r_{OH^-}$ were included for H^+ and OH^- according to water dissociation, while $r_i = 0$ for other ions. The electrode and membrane areas both have an area of A, and electrolyte volume is V, so the ratio $A/V=1/L$, where L is the distance between the electrode and CBL (electrode-CBL). The electrode-CBL distance is the difference between the electrode-membrane distance (3.7 cm), which is measured, and the CBL length (0.02 cm), which is estimated based on the literature.[25] Because the CBL thickness is two orders of magnitude less than the electrode-CBL distance, and therefore negligible, the electrode-membrane distance is defined as L = 3.7 cm. The current density was fixed at the anode boundary Γ_a as i_a =10 mA cm^{-2}, and the electrolyte potential was fixed at the cathode boundary Γ_c as φ = 0 V (as reference potential).

Internal boundary conditions have to be assigned too. On the interface connecting the membrane support with the anolyte Γ_{as}, continuity of potential and ion current, as well as concentrations and fluxes for all ions hold. On the active layer interfaces (Γ_{sm} and Γ_{cm}) however, partition conditions were set for concentrations and potential to influence ion permeance into the active layer, while ion fluxes and current must remain continuous. The concentration of ion i inside the membrane $c_{m,i}$ is related to its concentration outside in the water $c_{w,i}$ by $c_{m,i} = c_{w,i}K_i$. The partition coefficient K_i is the result of different effects, but we included Donnan partitioning as a function of the potential difference inside/outside the membrane, $\Phi_{D,i} = \exp\left(-z_i F \Delta\varphi / RT\right)$, and a lumped coefficient Φ_i for other effects (e.g., steric, dielectric), so that $K_i = \Phi_i \Phi_{D,i}$.[12, 14] Additionally, Φ_i was set to be the same value for all ions to simplify the number of fitting

parameters. By eliminating differences in size-based partitioning between the ions, we can analyze the importance of using these individual partitioning coefficients to describe selective ion transport across the TFC membranes in an induced electric field.

Initial Conditions. The initial electrolyte concentrations used for model calibration were 600 mM of $NaClO_4$ in the anolyte and 600 mM of KNO_3 in the catholyte with an initial pH of 5.7. Thus, for example, the initial values were $c_{0,Na^+} = c_{0,ClO_4^-} = 600$ mM, $c_{0,K^+} = c_{0,NO_3^-} = 0$, $c_{0,H^+} = 10^{-\mathrm{pH}}$, $c_{0,OH^-} = \frac{K_\mathrm{w}}{c_{0,\mathrm{H}^+}}$ for concentrations on the anolyte boundary Γ_a and domains Ω_a and Ω_s. Accordingly, $c_{0,Na^+} = c_{0,ClO_4^-} = 0$, $c_{0,K^+} = c_{0,NO_3^-} = 600$ mM for Γ_c and Ω_c. A zero initial electrolyte potential was set everywhere.

Model parameters. Values for the model parameters were obtained from literature for: diffusion coefficients[26-29], membrane layer thicknesses[22, 23], partitioning for H^+ and OH^-[24], and membrane charge density[16, 24], while boundary layer thicknesses was estimated from correlations and literature.[25] Operational parameters (initial concentrations, pH, current density) were measured. The diffusion effectiveness for the active (ε_a) and support (ε_s) membrane layers, and a single partition coefficient for all salt ions (Φ_i) were the three parameters used to fit the solution friction model to ion transport data (Table 1).

Model solution and validation. The model was solved for a 2 h period with an ultra-fine mesh in the membrane layers (20 nm in active layer, 0.5 μm in the support), and a fine mesh in the CBL (10 μm). The model was fit using the experimental transport data obtained during electrolysis with 600 mM electrolytes and a set constant current density of 10 mA cm^{-2}. To verify the model capability in predicting ion transport at different electrolyzer conditions, the set current density and initial electrolyte concentrations were changed according to new experimental conditions: (i) i_a increased to 14 mA cm^{-2}; (ii) initial electrolyte concentrations increased to 800 and 1000 mM in both electrolytes (i_a=10 mA cm^{-2}); (iii) at i_a=14 mA cm^{-2}, the electrolyte concentrations of 600, 800 and 1000 mM. In all cases, the initial pH was kept constant at 5.7.

Sensitivity analysis. A sensitivity analysis was conducted on some parameters taken from literature to determine whether deviations from these assumptions significantly influence ion crossover. The CBL thickness was varied from 50-300 μm, membrane backbone thickness from 100-150 μm, active layer thickness from 100-150 nm, and the membrane charge from 0-600 mM, all based on reasonable ranges from literature. [23, 25, 30].

Table 1. Model parameters, base case values.

Parameter	Description	Value	Unit	Source/Notes
	Geometry			
L	Distance electrode-membrane	3.7	cm	measured
L_a, L_c	Concentration boundary layer thickness	200	μm	[25]
L_s	Support layer thickness	150	μm	[23]
L_m	Active layer thickness	150	nm	[22]
	Mass transport			
D_i	Diffusion coefficients in water		$m^2\ s^{-1}$	20 °C
	Na^+	1.3×10^{-9}		[26]
	NO_3^-	1.7×10^{-9}		[27]
	K^+	2.0×10^{-9}		[26]
	ClO_4^-	1.8×10^{-9}		[28]
	H^+	9.3×10^{-9}		[29]
	OH^-	5.3×10^{-9}		[26]
ε_a	Membrane active layer diffusion effectiveness factor	0.001	-	fitted
ε_s	Membrane support layer diffusion effectiveness factor	0.015	-	fitted
Φ_i	Steric and dielectric partitioning		-	
	$Na^+, NO_3^-, K^+, ClO_4^-$	0.25		fitted
	$H^+,\ OH^-$	1		[16]
X	Membrane negative charge density	400	mM	[24]
	Aqueous equilibria			
K_w	Water equilibrium constant	1×10^{-14}	$mol^2\ L^{-2}$	
k_w	Water association rate constant	1×10^{-4}	$mol\ m^{-3}\ s^{-1}$	arbitrary value ensuring near equilibrium
	Operation			
i_a	Applied current density	10	$mA\ cm^{-2}$	measured
$c_{0,a}, c_{0,c}$	Initial concentrations anolyte ($NaClO_4$) / catholyte (KNO_3)	600	mM	measured
pH_0	Initial pH in anolyte / catholyte	5.7	-	measured
	Others			
T	Temperature	293.15	K	measured
R	Gas constant	8.3145	$J\ mol^{-1}\ K^{-1}$	
F	Faraday constant	96485	$C\ mol^{-1}$	

RESULTS AND DISCUSSION

Ion crossover used as baseline data

At the set current density of 10 mA cm^{-2} a relatively large electrolyte potential gradient developed across the reactor, which promoted the transport of Na^+ across the membrane into the catholyte and NO_3^- into the anolyte. In contrast, the transport of K^+ and ClO_4^- across the membrane was minimal, due to their diffusion in the direction opposite to the applied electric field. As a result, the final experimentally measured concentrations of Na^+ (63.5 ± 3.9 mM) and NO_3^- (59.6 ± 1.6 mM) were two orders of magnitude higher than the final concentrations of K^+ (0.4 ± 0.2 mM) and ClO_4^- (0.2 ± 0. 01 mM) after 2 hours of operation. The anolyte chamber rapidly became acidic due to H^+ generation by the OER, with a final pH of 0.9, and the pH in the catholyte chamber rapidly became basic due to OH^- generation by the HER, with a final pH of 13.3.

Model calibration

The model was calibrated using three fitting parameters ($\varepsilon_a, \varepsilon_s, \Phi$) and the other model parameters (Table 1) based on the ion crossover measured at the set current density of 10 mA cm^{-2} and electrolyte conditions of 600 mM. The fitted non-dimensional parameters were: ε_a = 0.001, the active layer transport effectiveness factor, ε_s = 0.015 the support layer effectiveness factor (clumping both polysulfone support and polyester backbone), and Φ = 0.25 steric/dielectric partitioning factor for all salt ions. Model agreement was based on the fit between the experimental data for the transport of the main charge carriers across the TFC membrane and the model prediction during the initial 120 minutes of electrolysis (Figure 2a). Initial fitting parameters were selected based on previous modeling of ion transport across polyamide layers[14], and adjustments were made to these parameters to obtain a better fit. The model was optimized with root mean square error values of 6.1 mM for Na^+ and 6.4 mM for NO_3^-. Additional membrane characterization and minimization of fitting parameters could be done in the future to further refine the fitting parameters by using a larger set of data for calibrating these models.

Model simulation using the parameters in Table 1 showed good agreement with the ion crossover results, with only slight deviations between the model and experimental data despite the use of a limited number of fitting parameters. The agreement of the model and experimental results indicated that the electric field was the dominant factor in driving the major salt ions across the PA active layer. Using the fit model, the diffusion and migration fluxes in and around the membrane could be broken down into their individual components (Figures S4a and S4b). While diffusion flux was higher inside the active layer, the migration flux dominated the major ion transport in their initial compartments and across most of the backbone. This fit of the major salt ions for balancing charge (Na^+ and NO_3^-) was possible without having to include individual size-based partition coefficients or friction factors for individual ions.

A sensitivity analysis of the active layer thickness L_m, support layer thickness L_s, and boundary layer thickness, L_a and L_c indicated that changing these parameters between the upper and lower bounds of a reasonable range for each value based on the literature revealed that there were only very small changes in ion transport (Figure S5, S6, and S7). The largest change for the main charge carriers (Na^+, NO_3^-) was due to varying the active layer thickness. Increasing the active

layer from 100 nm to 200 nm increased Na^+ ion crossover by 6.7% (from 63.8 mM to 68.1 mM) and decreased NO_3^- crossover by 10%) (from 75.1 mM to 67.2 mM). In comparison, changing the backbone thickness from 100 µm to 250 µm caused a 3.8% change in Na^+ crossover and a 4.4% change in NO_3^- crossover, while changing the boundary layer thickness from 50 µm to 300 µm caused a 1.2% change in Na^+ and a 1.8% change in NO_3^-.

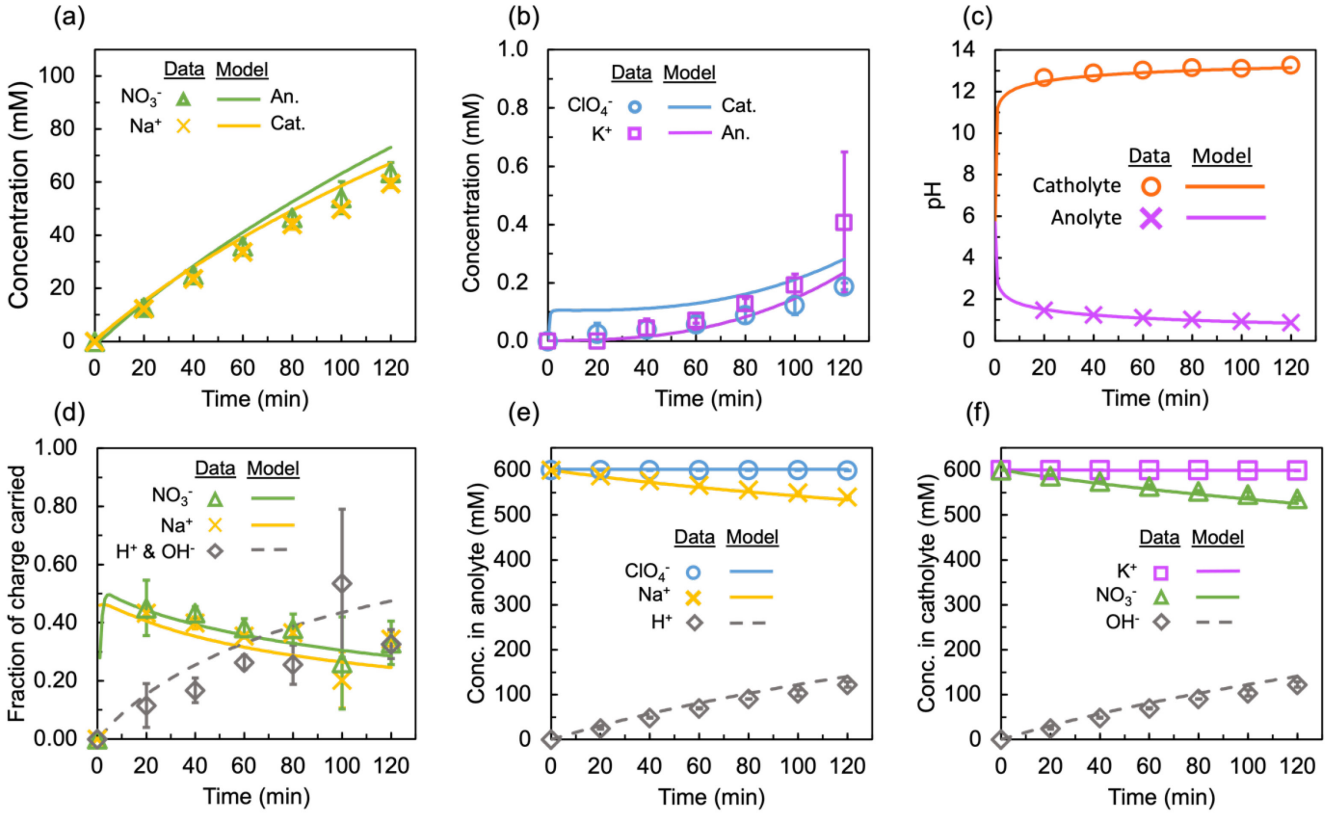

Figure 2. (a) Salt ion transport across the TFC membrane over 120 minutes of electrolysis in the catholyte (Cat) and anolyte (An). (b) Concentration of K^+ and ClO_4^- transported across the membrane. Note the different scales of the y-axis on figures a and b. (c) Bulk pH in the anolyte and catholyte during electrolysis. (d) The fraction of charge carried across the TFC membrane by major salt ions (Na^+ and NO_3^-) and water ions. (e) the bulk concentration of ClO_4^-, Na^+, and H^+ calculated via electroneutrality with the ion crossover data and projected by the model. (f) Bulk concentration of K^+, NO_3^-, and OH^- in the catholyte during electrolysis.

The change in the average concentrations of H^+ and OH^- in the two chambers based on pH over time was in good agreement with the model predictions (Figure 2c). Using the measured and modeled ion transport data, the fraction of current carried across the TFC membrane by each ion was calculated to compare the relative importance of salt versus water ion transport in maintaining the set current density (Figure 2d). Salt ions initially carried most of the charge across the membrane in these tests, but the fraction of charge carried by water ions substantially increased over time. A concentration profile of the salt ions across the CBLs, backbone, and active layer is presented in the SI, as well as the potential profile across the system (Figure S3a

and Figure S3c). The concentration profile of Na^+ across the system is plotted at several time positions to demonstrate how transport changes over time in the SI (Figure S3d)

While the experimental results and the model produced good agreement in the concentrations of H^+ based on pHs (0.9 for the anolyte, and 13.2 for the catholyte according to the model), the final concentrations of H^+ in the anolyte and OH^- were more noticeably different when compared on a linear scale. By using the ion transport data, the linear concentration of water ions in the bulk solutions could be calculated according to electroneutrality. The concentration of H^+ in the anolyte increased from essentially zero (0.002 mM) at the initial neutral pH to 122 mM ± 6 mM according to experimental data and 141 mM according to the model (Figure 2e). The same increase in OH^- concentration was observed in the catholyte, as H^+ and OH^- are generated at the same rate at the electrodes (Figure 2f). These increases in the concentrations of the water ions in the chambers enabled more current to be carried across the membrane by these ions as their concentrations approached those of the salt ions. The final fraction of charge carried by water ions was 33% ± 5% based on the final pH, compared to 47% by the model. K^+ and ClO_4^- combined accounted for <1 mM of ion transport across the membrane after 120 minutes of electrolysis (Figure 2d). These ions transport across the membrane in the opposite direction of the current density in such small concentrations they can be considered minor current contributors to the system. The ion chromatography methods used were optimized for the measurement of the major ions in the system rather than the dilute minor ions. Because neither ion participates in unwanted side reactions at either the anode or cathode (ClO_4^- is fully oxidized, and the reduction reaction is not known to compete with hydrogen evolution), differences between the experimental data and model simulations were not a concern due to the focus on the transport of chloride or nitration ions.[31] Likely better agreement between the model and data could be obtained by adjusting individual ion parameters, but the goal here was to minimize fitting parameters needed to reproduce the main characteristics of the system.

NO_3^- and Na^+ transport across the membrane is limited to what is required to maintain the set current density, although NO_3^- permeation in the current configuration is higher than desired for larger-scale electrolysis. Additional membrane and electrolyzer modifications are being studied to decrease Cl^- permeation to the anode. For example, adding polyamide active layers to both sides of the TFC membrane successfully reduced Cl^- permeation from the catholyte to the anolyte by 53% during electrolysis with a zero gap electrolyzer.[13] Additionally, the zero-gap electrolyzer configuration enables lower salt ion permeation in comparison to the batch electrolyzer used here with a membrane-electrode distance of 3.7 cm. The same amount of total salt ion transport after two hours in the batch electrolyzer occurs after 6 hours in the zero-gap electrolyzer.[12] The smaller electrode-membrane distance in the zero-gap configuration enables a higher percentage of charge to be carried by water ions generated at the electrodes, while water ions are forced to first migrate across the electrolyte chambers in the batch configuration.[13]

Model validation by changing electrolyte concentrations

The crossover of salt ions predicted by the model was compared to experimental results using two additional initial electrolyte concentrations of 800 mM and 1000 mM at a set current density of 10 mA cm^{-2}. When the initial electrolyte concentrations in both chambers were increased to 800 mM and 1000 mM, the model predicted only slightly different amounts of total salt ion crossover than those measured. For a 67% increase in electrolyte concentration (600 to 1000

mM) the model predicted an 18% increase in NO_3^- crossover compared to the observed 17% ± 2% crossover. For Na^+ the model predicted 11% crossover, compared to 18% ± 3% measured (Figure 3).

The final transport of K^+ and ClO_4^- ions predicted by the model was within 2 mM of the total crossover measured. The final value of K^+ transport predicted for an 800 mM electrolyte was 1.5 mM, which is the same as that obtained in experiments, while the final crossover predicted for the 1000 mM electrolyte case was 3.8 mM compared to the measurement of 2.6 ± 0.3 mM. The final transport of ClO_4^- predicted by the model for the 800 mM electrolyte case was 1.5 mM compared to a measured value of 0.6 ± 0.3 mM and for the 1000 mM case was 3.7 mM compared to the measured value of 1.8 ± 0.6 mM. While these are large percentage changes, it is considered here that a better fit of these minor ions through introducing additional parameters is not needed because these ions carry little charge across the membrane.

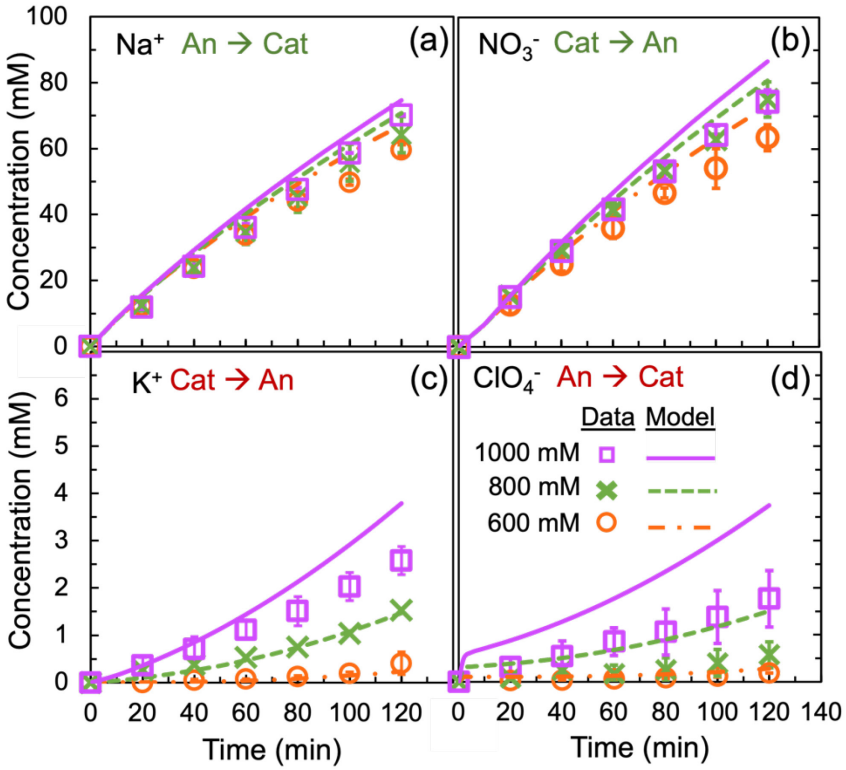

Figure 3. The experimentally measured and modeled transport of (a) Na^+ (b) NO_3^- (c) K^+ and (d) ClO_4^- ions across the membrane during electrolysis with increasing initial anolyte and catholyte concentrations. Green text indicates ions moving in the same direction of the potential gradient across the membrane (positively charged ions moving towards the negatively charged electrode, or negatively charge ions moving towards a positively charged electrode) and red text indicates ions moving in the opposite direction of the potential gradient across the membrane (positively charged ions moving towards the positively charged electrode and negatively charged ions moving towards the negatively charged electrode).

Increasing the salt concentration resulted in a decrease in the amount of charge carried by water ions (Figure S8). Water ions accounted for 33 ± 5% of current transport with a 600 mM

electrolyte but decreased to 27 ± 13% with an 800 mM electrolyte and 24 ± 4% with a 1000 mM electrolyte. Since the current density was the same while the salt concentration was increased, the ratio of salt ions to water ions in solution increased, resulting in more salt ions carrying charge across the membrane.

Impact of current density on ion transport

Increasing the current density will require a corresponding increase in total ion migration across the membrane. The main charge carrier transport was predicted reasonably well by the model when the current density was increased from 10 to 14 mA cm^{-2} with an electrolyte concentration of 600 mM. The predicted crossover of NO_3^- into the anolyte after 120 minutes was 90.7 mM compared to the 78.5 ± 2.2 mM observed, and the predicted crossover of Na^+ into the catholyte was 87.8 mM compared 86.9 ± 1.4 mM (Figure 4a and 4b). Increasing the current density by 40% caused a 33.7% increase in total crossover of main salt ions, as salt ions are the main charge carriers across the membrane. Additional simulations were done using 800 mM and 1000 mM electrolytes with similarly good agreement between the model and data (Figure S9 and S10). Increasing the current density resulted in an increased fraction of charge carried by water ions and decreased fraction of charge carried by salt ions predicted by the model at the end of 120 minutes of electrolysis (Figure S11). Although the higher current density caused more salt ion transport, it also resulted in a larger rate of water ions generated at the electrodes. The water ions are preferable charge carriers across the membrane, so increasing the ratio of water ions to salt ions in solution caused a higher fraction of charge to be carried by water ions.

The differences in minor ion transport data and model predictions after 120 minutes of electrolysis were within 0.7 mM for K^+ and 0.5 mM for ClO_4^- with a current density of 14 mA cm^{-2} (Figure 4c, 4d). At the higher current density, the model predicted final crossover of 0.02 mM for K^+ and 0.05 mM for ClO_4^-, while K^+ was experimentally measured to have 0.7 ± 0.5 mM and ClO_4^- had 0.4 ± 0.1 mM of total transport. The model predicted that increasing the current density would decrease the amount of minor ions crossing over the membrane. However, the experimental trend was the opposite, showing a higher transport of K^+ and ClO_4^- across the

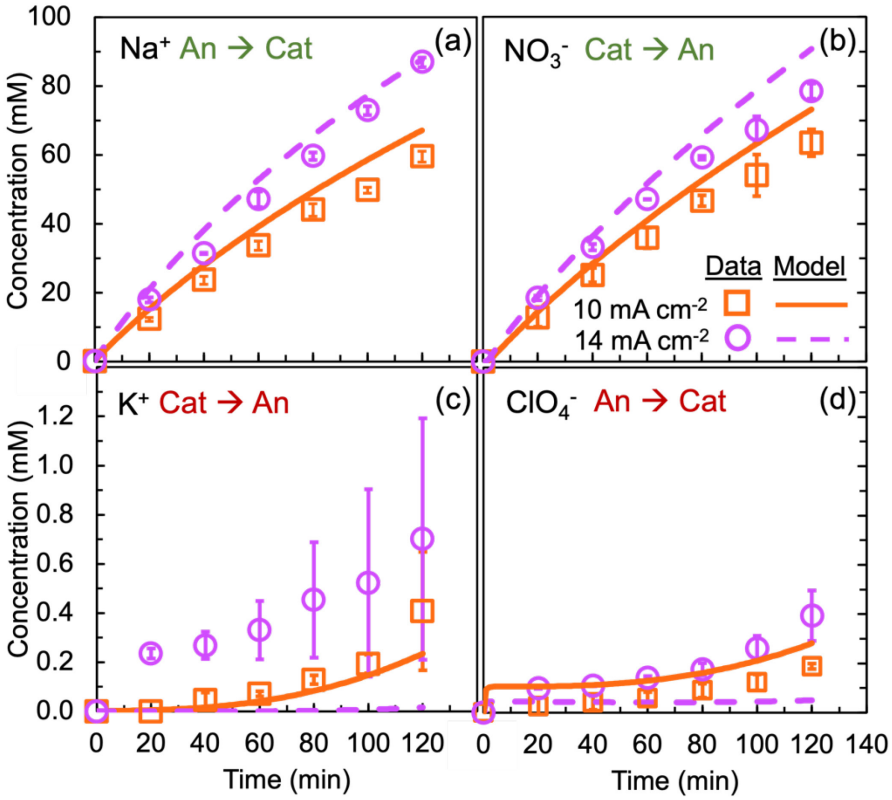

Figure 4. The experimentally measured and modeled transport of (a) Na^+ (b) NO_3^- (c) K^+ and (d) ClO_4^- ions across the membrane during electrolysis with increasing current density and initial anolyte and catholyte concentrations of 600 mM. Green text indicates ions moving in the same direction of the potential gradient and red text indicates ions moving in the opposite direction of the potential gradient.

membrane at higher current densities. Determining whether this discrepancy is meaningful or merely a result of slight inaccuracies in measuring ClO_4^- and K^+ ion crossover is challenging, as ion chromatography techniques were optimized for the measurement of the major ions in the system, rather than the dilute minor ions. Additional electrolysis simulations and experiments done with initial conditions of 800 mM and 1000 mM electrolytes can also be found in the SI (Figure S7 and S8).

Relative insignificance of membrane charge and Donnan partitioning on ion crossover

The model was used to predict the impact of membrane charge on ion crossover. Increasing the membrane charge from –400 to –600 mM was predicted to increase the crossover of Na^+ ions by 5% (total of 3.5 mM) and decrease NO_3^- ion crossover by 9% (6.3 mM) (Figure 5a and Figure 5b). In the absence of a charge on the membrane (0 mM), Na^+ was predicted to decrease by 7%

(4.4 mM), and NO_3^- was predicted to increase by 11% (7.7 mM). Making the membrane more negatively charged should have increased the Donnan partitioning effect, which would have decreased NO_3^- crossover, consistent with the model's predicted decrease of this ion.

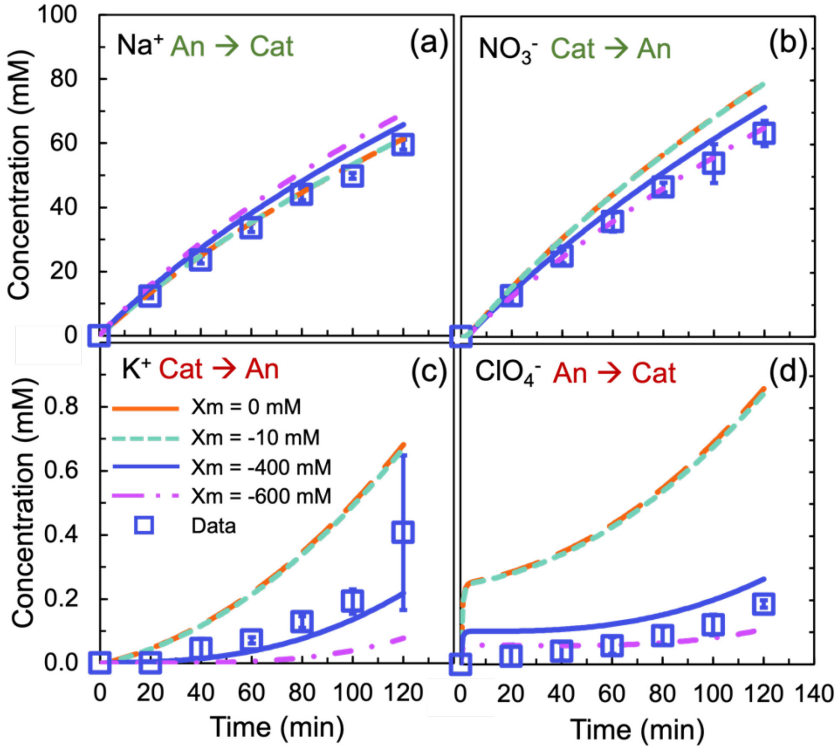

Figure 5. Concentration measured in adjacent chamber of (a) Na^+ (b) NO_3^- (c) K^+ and (d) ClO_4^- during electrolysis when the membrane charge is changed between -600 mM and 0 mM. Green arrows indicate ions moving in the same direction as the potential gradient, and red arrows indicate ions moving in the opposite direction of the potential gradient.

Previous studies using Rutherford backscattering spectroscopy and electron impedance spectrometry have suggested the maximum negative charge of a fully aromatic polyamide membrane might be somewhere between –400 mM or –600 mM depending on the membrane at pH values greater than 13.[24, 32] Using the COMSOL simulation to sweep the membrane charge from 0 mM to -600 mM predicted that the ratio of Na^+ versus NO_3^- transporting across the membrane changed, although the total major salt ion transport across the membrane remained relatively constant (141 mM with 0 mM charge and 135 mM with -600 mM charge). One potential explanation for the decrease in NO_3^- crossover is because the negatively charged membrane resisted the transport of this anion due to increased Donnan partitioning at the membrane interface. Conversely, more Na^+ ions might have been partitioned into the negative membrane to maintain electroneutrality, resulting in higher flux of Na^+ into the catholyte.[33] For the other two ions (K^+ and ClO_4^-) where the direction of the electric field is not driving their transport across the membrane changing the membrane charge from 0 mM to 600 mM caused less than a 1 mM change in their overall transport across the membrane.

These simulation results corroborate with previous experimental ion transport results in a zero-gap electrolyzer which demonstrated that membrane charge could be used to tune the ratio of salt ions transported but could not be used to increase the total fraction of charge carried by water ions.[13] Recent studies have debated the impact of polyamide membrane charge on water purification systems using typical reverse osmosis and nanofiltration membranes, suggesting the RBS and EIS studies might not be capturing the effective membrane charge that exists during operation in high salinity and pH solutions.[34] Whether or not the membrane is truly highly charged in this electrolyzer set-up with high pH values is unclear based on the simulation results. The differences in ion transport due to a higher negatively charged membrane versus an uncharged membrane are small enough to be fixed by slightly changing other fitting parameters. In comparison to the set current density, which dictated a flux of salt ions across the membrane, the membrane charge was relatively insignificant in controlling salt ion transport across the membrane.

Insights into water ion transport through the TFC membrane

The model was used to predict spatial changes in pH across the membrane, as pH changes within the two membrane layers would be difficult to measure. The pH data is presented over a general schematic of the reactor to provide some spatial reference points to make the data easier to interpret. The pH was indicted to be constant across the concentration boundary layers in the electrolyte chambers, consistent with the construction of the model to have diffusion coefficients like those in water, resulting in fast diffusion across these regions (Figure 6). While there might be linear concentration gradients across these concentration boundary layers, small changes in H^+ and OH^- concentrations on a linear scale do not translate to large pH changes on a log scale. The pH in the active layer was calculated to be nearly constant at pH=12.6. Thus, the active layer was highly alkaline, and at this pH all the carboxylic acid groups in the membrane would be deprotonated, causing the membrane to have a negative charge somewhere between –400 to –

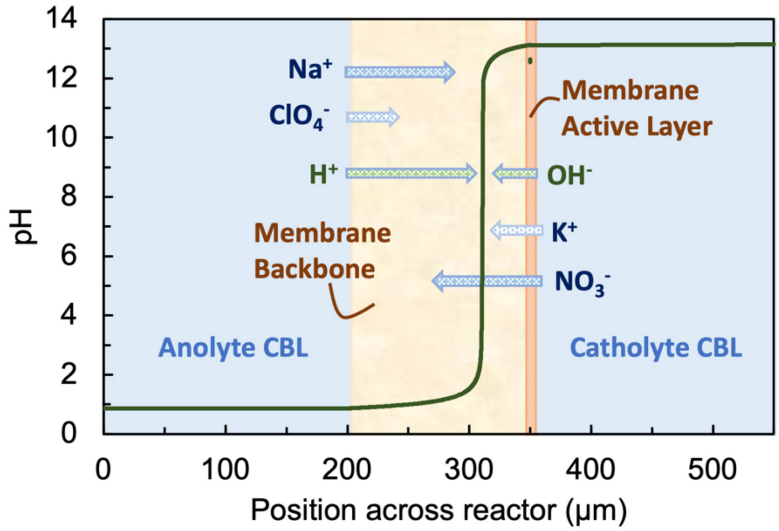

Figure 6. pH across model, which includes concentration boundary layers, the membrane backbone, and membrane active layer.

600 mM.[24] The model predicted a steep pH gradient in the support layer, nearer to the active layer (cathode side) than the anolyte, where H^+ meet OH^- and essentially instantaneously combine in the water association reaction (Figure 6). At higher current densities typically used

industrially, this pH gradient would be more difficult to compute because the flux of H^+ and OH^- through the membrane will be larger, so more water association would be occurring. More computational power (finer meshes, smaller step sizes, different assumptions, etc.) will be required for future studies at industrial level current densities but these simulations will provide necessary insights into salt and water ion transport.

Short term stability tests (5 h) indicated that the polyamide membranes were stable for the pH conditions in these experiments, and manufacturer spec sheets suggest these membranes are stable for short periods of time in pH conditions from 1 to 13.[35] The purpose of this work is validating the model during the initial electrolysis period with extreme pH changes, so the long-term stability of the membrane does not impact the results here. Future work could study long term membrane stability during electrolysis and examine different membrane modifications to improve stability.

Implications

In this study, a solution friction transport model was fit to ion transport data across a polyamide membrane during electrolysis using minimal fitting parameters in the active layer. Specifically, the same steric and dielectric partition coefficient, as well as friction coefficient, was used for all salt ions through the membrane. Without accounting for size differences in salt ions other than their different diffusion coefficients, the fit model was successfully validated against the transport data of main charge carriers across the membrane when the current density and electrolyte concentrations were increased. A set current density required a flux of charge across the membrane, and water ions existed in solution at much lower concentrations than salt ions, so salt ions consistently carried most of the charge across the membrane. Increasing the membrane charge changed the ratio of salt ions carrying charge across the membrane but did not decrease the total amount of salt ions transported. NO_3^- crossover, which is indicative of Cl^- crossover, can be reduced in saltwater electrolysis by increasing the negative charge of the membrane. Additionally, salt ion transport is controlled by the set current density, so modifying the electrolyzer conditions to change the main charge carriers in conjunction with membrane modifications can decrease Cl^- transport further.

■ ASSOCIATED CONTENT

Supporting Information: Pictures of experimental apparatus used; concentration and potential profiles across the reactor and membrane parts generated by the model; flux profiles, including the separation of diffusion and migration fluxes, across the reactor generated by the model; example calculation of fraction of charge carried by salt ions; results of parametric sweeps of values estimated from literature; additional model validation of ion transport with a set current density of 14 mA cm^{-2} and increasing electrolyte concentrations; and both model and experimental results for the fraction of charge carried by salt and water ions with increasing electrolyte concentration and increasing current density (PDF).

Notes

The authors declare no competing financial interest.

■ ACKNOWLEDGMENTS
This research was funded by National Science Foundation grant CBET-2027552 and Penn State University through the Stan and Flora Kappe endowment.

References

(1) *Global Hydrogen Review 2023*; International Energy Agency, Paris, 2023. https://www.iea.org/reports/global-hydrogen-review-2023 (accessed 2024-05-30).
(2) *Electrolysers*; International Energy Agency, Paris, 2023. https://www.iea.org/reports/electrolysers (accessed 2024-05-30).
(3) Boyano, A.; Blanco-Marigorta, A. M.; Morosuk, T.; Tsatsaronis, G. Exergoenvironmental analysis of a steam methane reforming process for hydrogen production. *Energy* **2011**, *36* (4), 2202-2214. DOI: 10.1016/j.energy.2010.05.020.
(4) Esposito, D. V. Membraneless electrolyzers for low-cost hydrogen production in a renewable energy future. *Joule* **2017**, *1* (4), 651-658. DOI: 10.1016/j.joule.2017.07.003.
(5) Lee, H.; Lee, B.; Byun, M.; Lim, H. Economic and environmental analysis for PEM water electrolysis based on replacement moment and renewable electricity resources. *Energy Conversion and Management* **2020**, *224*, 113477. DOI: 10.1016/j.enconman.2020.113477.
(6) Gao, F.-Y.; Yu, P.-C.; Gao, M.-R. Seawater electrolysis technologies for green hydrogen production: Challenges and opportunities. *Current Opinion in Chemical Engineering* **2022**, *36*, 100827. DOI: 10.1016/j.coche.2022.100827.
(7) Guo, J.; Zheng, Y.; Hu, Z.; Zheng, C.; Mao, J.; Du, K.; Jaroniec, M.; Qiao, S.-Z.; Ling, T. Direct seawater electrolysis by adjusting the local reaction environment of a catalyst. *Nat. Energy* **2023**, *8* (3), 264-272. DOI: 10.1038/s41560-023-01195-x.
(8) Shi, L.; Rossi, R.; Son, M.; Hall, D. M.; Hickner, M. A.; Gorski, C. A.; Logan, B. E. Using reverse osmosis membranes to control ion transport during water electrolysis. *Energy Environ. Sci.* **2020**, *13* (9), 3138-3148. DOI: 10.1039/d0ee02173c.
(9) Dionigi, F.; Reier, T.; Pawolek, Z.; Gliech, M.; Strasser, P. Design criteria, operating conditions, and nickel-iron hydroxide catalyst materials for selective seawater electrolysis. *Chemsuschem* **2016**, *9* (9), 962-972. DOI: 10.1002/cssc.201501581.
(10) Petersen, R. J. Composite reverse-osmosis and nanofiltration membranes. *J. Membr. Sci.* **1993**, *83* (1), 81-150. DOI: 10.1016/0376-7388(93)80014-O.
(11) Taylor, R.; Shi, L.; Zhou, X.; Rossi, R.; Picioreanu, C.; Logan, B. E. Electrochemical and hydraulic analysis of thin-film composite and cellulose triacetate membranes for seawater electrolysis applications. *J. Membr. Sci.* **2023**, *679*, 121692. DOI: 10.1016/j.memsci.2023.121692.
(12) Zhou, X.; Shi, L.; Taylor, R. F.; Xie, C.; Bian, B.; Picioreanu, C.; Logan, B. E. Relative insignificance of polyamide layer selectivity for seawater electrolysis applications. *Environ. Sci. Technol.* **2023**, *57* (39), 14569-14578. DOI: 10.1021/acs.est.3c04768.
(13) Zhou, X.; Taylor, R. F.; Shi, L.; Xie, C.; Bian, B.; Logan, B. E. Reducing chloride ion permeation during seawater electrolysis using double-polyamide thin-film composite membranes. *Environ. Sci. Technol.* **2024**, *58* (1), 391-399. DOI: 10.1021/acs.est.3c07248.
(14) Wang, L.; Cao, T. C.; Dykstra, J. E.; Porada, S.; Biesheuvel, P. M.; Elimelech, M. Salt and water transport in reverse osmosis membranes: Beyond the solution-diffusion model. *Environ. Sci. Technol.* **2021**, *55* (24), 16665-16675. DOI: 10.1021/acs.est.1c05649.

(15) Geraldes, V.; Brites Alves, A. M. Computer program for simulation of mass transport in nanofiltration membranes. *J. Membr. Sci.* **2008**, *321* (2), 172-182. DOI: 10.1016/j.memsci.2008.04.054.
(16) Zhang, L.; Hamelers, H. V. M.; Biesheuvel, P. M. Modeling permeate pH in RO membranes by the extended Donnan steric model. *J. Membr. Sci.* **2020**, *613*. DOI: 10.1016/j.memsci.2020.118511.
(17) Biesheuvel, P. M.; Zhang, L.; Gasquet, P.; Blankert, B.; Elimelech, M.; van der Meer, W. G. J. Ion selectivity in brackish water desalination by reverse osmosis: Theory, measurements, and implications. *Environ. Sci. Tech. Let.* **2020**, *7* (1), 42-47. DOI: 10.1021/acs.estlett.9b00686.
(18) Castaño Osorio, S.; Biesheuvel, P. M.; Spruijt, E.; Dykstra, J. E.; van der Wal, A. Modeling micropollutant removal by nanofiltration and reverse osmosis membranes: Considerations and challenges. *Water Res.* **2022**, *225*, 119130. DOI: 10.1016/j.watres.2022.119130.
(19) Zubair, M. M.; Saleem, H.; Zaidi, S. J. Recent progress in reverse osmosis modeling: An overview. *Desalination* **2023**, *564*, 116705. DOI: 10.1016/j.desal.2023.116705.
(20) Zhang, G.; Sun, S.; Yang, D.; Dodelet, J.-P.; Sacher, E. The surface analytical characterization of carbon fibers functionalized by H2SO4/HNO3 treatment. *Carbon* **2008**, *46* (2), 196-205. DOI: 10.1016/j.carbon.2007.11.0027.
(21) Zhong, C.; Deng, Y.; Hu, W.; Qiao, J.; Zhang, L.; Zhang, J. A review of electrolyte materials and compositions for electrochemical supercapacitors. *Chemical Society Reviews* **2015**, *44* (21), 7484-7539, 10.1039/C5CS00303B. DOI: 10.1039/C5CS00303B.
(22) Chu, K. H.; Mang, J. S.; Lim, J.; Hong, S.; Hwang, M.-H. Variation of free volume and thickness by high pressure applied on thin film composite reverse osmosis membrane. *Desalination* **2021**, *520*, 115365. DOI: 10.1016/j.desal.2021.115365.
(23) Liu, F.; Wang, L.; Liu, Q.; Deng, B. A review: the effect of the microporous support during interfacial polymerization on the morphology and performances of a thin film composite membrane for liquid purification. *Rsc Adv* **2019**, *9*, 35417-35428. DOI: 10.1039/C9RA07114H.
(24) Coronell, O.; González, M. I.; Mariñas, B. J.; Cahill, D. G. Ionization behavior, stoichiometry of association, and accessibility of functional groups in the active layers of reverse osmosis and nanofiltration membranes. *Environ. Sci. Technol.* **2010**, *44* (17), 6808-6814. DOI: 10.1021/es100891r.
(25) Li, M.; Xiang, Z.; Guo, J.; Zhang, N.; Zheng, H.; Li, X.; Hao, Y. Direct measurement of boundary layer thickness on ion-exchange membrane surfaces during reverse electrodialysis. *Sustainable Energy & Fuels* **2023**, *7* (13), 3060-3066, 10.1039/D3SE00404J. DOI: 10.1039/D3SE00404J.
(26) Samson, E.; Marchand, J.; Snyder, K. A. Calculation of ionic diffusion coefficients on the basis of migration test results. *Materials and Structures* **2003**, *36* (3), 156-165. DOI: 10.1007/BF02479554.
(27) Kreft, J. U.; Picioreanu, C.; Wimpenny, J. W.; van Loosdrecht, M. C. Individual-based modelling of biofilms. *Microbiology (Reading)* **2001**, *147* (Pt 11), 2897-2912. DOI: 10.1099/00221287-147-11-2897 From NLM.
(28) Heil, S.; Holz, M.; Kastner, T.; Weingärtner, H. Self-diffusion of the Perchlorate Ion in Aqueous Electrolyte Solutions Measured by 35-Cl NMR Spin-Echo experiments. *Journal of the Chemical Society Faraday Transactions* **1995**, *91*, 1877-1880. DOI: 10.1039/FT9959101877.
(29) Agmon, N. The Grotthuss mechanism. *Chemical Physics Letters* **1995**, *244* (5), 456-462. DOI: 10.1016/0009-2614(95)00905-J.

(30) Warnken, K. W.; Zhang, H.; Davison, W. Accuracy of the diffusive gradients in thin-films technique: Diffusive boundary layer and effective sampling area considerations. *Analytical Chemistry* **2006**, *78* (11), 3780-3787. DOI: 10.1021/ac060139d.
(31) Dresp, S.; Dionigi, F.; Klingenhof, M.; Strasser, P. Direct electrolytic splitting of seawater: Opportunities and challenges. *Acs Energy Lett.* **2019**, *4* (4), 933-942. DOI: 10.1021/acsenergylett.9b00220.
(32) Stolov, M.; Freger, V. Membrane charge weakly affects ion transport in reverse osmosis. *Environ. Sci. Tech. Let.* **2020**, *7* (6), 440-445. DOI: 10.1021/acs.estlett.0c00291.
(33) Fan, H.; Huang, Y.; Billinge, I. H.; Bannon, S. M.; Geise, G. M.; Yip, N. Y. Counterion Mobility in Ion-Exchange Membranes: Spatial Effect and Valency-Dependent Electrostatic Interaction. *ACS ES&T Engineering* **2022**, *2* (7), 1274-1286. DOI: 10.1021/acsestengg.1c00457.
(34) Blankert, B.; Huisman, K. T.; Martinez, F. D.; Vrouwenvelder, J. S.; Picioreanu, C. Are commercial polyamide seawater and brackish water membranes effectively charged? *Journal of Membrane Science Letters* **2022**, *2* (2), 100032. DOI: 10.1016/j.memlet.2022.100032.
(35) *FilmTech SW30XLE-400*; DuPont, 2022. https://www.dupont.com/content/dam/dupont/amer/us/en/water-solutions/public/documents/en/RO-FilmTec-SW30XLE-400-PDS-45-D00972-en.pdf (accessed 2024-05-30).